J Mater Sci: Mater Med (2010) 21:3171–3181
DOI 10.1007/s10856-010-4168-4

Evaluation of colloidal silica suspension as efficient additive for improving physicochemical and in vitro biological properties of calcium sulfate-based nanocomposite bone cement

Shokoufeh Borhan · Saeed Hesaraki · Shaghayegh Ahmadzadeh-Asl

Received: 4 January 2010 / Accepted: 7 October 2010 / Published online: 23 October 2010

Abstract In the present study new calcium sulfate-based nanocomposite bone cement with improved physicochemical and biological properties was developed. The powder component of the cement consists of 60 wt% α-calcium sulfate hemihydrate and 40 wt% biomimetically synthesized apatite, while the liquid component consists of an aqueous colloidal silica suspension (20 wt%). In this study, the above mentioned powder phase was mixed with distilled water to prepare a calcium sulfate/nanoapatite composite without any additive. Structural properties, setting time, compressive strength, in vitro bioactivity and cellular properties of the cements were investigated by appropriate techniques. From X-ray diffractometer analysis, except gypsum and apatite, no further phases were found in both silica-containing and silica-free cements. The results showed that both setting time and compressive strength of the calcium sulfate/nanoapatite cement improved by using colloidal silica suspension as cement liquid. Meanwhile, the condensed phase produced from the polymerization process of colloidal silica filled the micropores of the microstructure and covered rodlike gypsum crystals and thus controlled cement disintegration in simulated body fluid. Additionally, formation of apatite layer was favored on the surfaces of the new cement while no apatite precipitation was observed for the cement prepared by distilled water. In this study, it was also revealed that the number of viable osteosarcoma cells cultured with extracts of both cements were comparable, while silica-containing cement increased alkaline phosphatase activity of the cells. These results suggest that the developed cement may be a suitable bone filling material after well passing of the corresponding in vivo tests.

S. Borhan · S. Hesaraki (✉) · S. Ahmadzadeh-Asl
Ceramics Department, Materials and Energy Research Center (MERC), P.O. Box 14155-4777, Tehran, Iran
e-mail: s-hesaraki@merc.ac.ir

1 Introduction

Synthetic and natural bone graft substitutes with different chemical formulations, resorption rates and shapes are traditionally considered as osteoconductive materials [1]. Hydroxyapatite bone graft substitutes, corals, calcium phosphates and calcium sulfates have been successfully used in the treatment of a variety of bone defects. The selection of the reconstructive material type is based on many factors including the size and location of the defect, the handling properties and ability of the material for delivering to the surgical site [2, 3].

Bioceramic cements, such as calcium phosphates and calcium sulfates, exhibit individual properties such as low temperature self-setting behavior, injectability, moldability to defects with complex configuration and the possibility for drug-loading devices [4, 5].

Calcium sulfate cements are biocompatible and osteoconductive synthetic grafts with a long clinical history in treating bone defects such as alveolar bone loss, maxillary sinus augmentation and periodontal diseases [6–8]. The presence of calcium sulfate in bone defects did not inhibit the normal bone healing process and did not create additional complications [9]. Despite of all these advantages, calcium sulfate cements represent too fast resorption rate to provide an appropriate support for the newly formed bone [10]. This leads to the formation of an immature bone in the site of defect. Slightly transient cytotoxicity of calcium sulfate caused inflammatory reaction in host tissues has also been reported by some authors [11, 12].

Table 1 Chemical formulation of different bone cements investigated in this study

Code of specimen	Powder phase	Liquid phase
C	CSH (100%)	Distilled water
C-H	CSH (60 wt%) + nanoapatite (40 wt%)	Distilled water
C-H-S20	CSH (60 wt%) + nanoapatite (40 wt%)	Suspension of 20 wt% nanosilica

To solve these problems, a biocompatible and osteoconductive phase such as hydroxyapatite [10, 13] or nanostructured apatite [14] has been incorporated into calcium sulfate cement/bulk formulations. It has been reported that dissolution rate, biocompatibility and controlled-releasing properties of calcium sulfate cements are improved by admixing 40–60 wt% hydroxyapatite filler [10, 13, 15].

Unfortunately, several drawbacks occur when an apatitic phase is incorporated into the calcium sulfate cement formulation to form composite bone cement. These disadvantages are long initial setting time, weak compressive strength and disintegration of cement structure when immersing in a physiologic solution.

In the present study, colloidal silica was used to improve the above mentioned drawbacks of calcium sulfate/apatite composite and to enhance its in vitro bioactivity and cell activity responses.

2 Materials and methods

2.1 Preparation of the cement components and pastes

In this work, pure calcium sulfate cement (C), nanocomposite cement of calcium sulfate and nanostructured apatite (C-H), and nanocomposite cement of calcium sulfate/nanostructured apatite/nanosilica were prepared and investigated. Calcium sulfate hemihydrate (CSH) that was used as reactive ingredient of the cements was purchased from Aldrich Company (India) and colloidal silica was prepared as an aqueous suspension of stabilized amorphous silica (Shiv Kripa, India). The particle size of colloidal silica measured with a zeta sizer device (Zeta-Sizer 3000HS) was about 60 nm.

The nanoapatite component of the cements with nanospindle shaped crystals was synthesized by using calcium phosphate cement reactants according to the method described previously [14]. Briefly, a mixture of 1 mol tetracalcium phosphate (produced base on the method described previously [16]) and 1 mol dicalcium phosphate dihydrate (Merck, Germany) was added to a solution of 6 wt% Na_2HPO_4 at a solid to liquid ratio of 3 g/ml and the obtained paste was left hardening. 100 g of the set product was then soaked in 1,000 ml of a simulated body fluid (SBF) solution which was prepared in accordance with the Kokubo specification [17]. After 7 days of soaking, the product was removed from the SBF, washed with distilled water, dried at room temperature and grounded by using a planetary mill at a rotating rate of 190 rpm for 2 h.

Various calcium sulfate-based cements were produced in this study by mixing a powder phase (P) with a liquid phase (L) at P/L ratio of 2.5 g/ml. Table 1 presents chemical formulation of various cements along with the code of each one. Note that the weight of nanosilica (the solid phase of silica suspension) was considered in calculating P/L ratio.

2.2 Characterization

2.2.1 Initial setting time

The initial setting time of the cements was recorded by a Gillmore needle according to the ASTM-C266-89 standard. Initial setting time is defined as the time that a light needle (113.4 g) with a tip diameter of 2.13 mm does not form a visible print onto the surface of the cement specimen.

2.2.2 Mechanical strength

The compressive strength of each cement formulation was measured as follow: The cement paste was poured into a Teflon mold to obtain cylindrical specimens with a height to diameter ratio of 2:1 (12 mm in height and 6 mm in diameter). The specimens were removed from the moulds after 4 h and incubated at 37°C and 100% humidity for 24 h. Compressive strength of the wet specimens was measured by using a universal testing machine (Zwick/Roell-HCR 25/400) at a crosshead speed of 1 mm/min.

2.2.3 Phase analysis

To estimate the phase composition of the cements, the hardened samples were dried at room temperature, grounded to fine powder and characterized by using the automated X-ray diffractometer (XRD) device (Philips PW3710) with Cu-K_α radiation. Data were collected from $2\theta = 10°–50°$ with a step size of 0.1 and a count time of 3 s/step. The XRD data were checked by using standard

patterns from international center for diffraction data (ICDD).

2.2.4 Structural groups

Chemical groups in the set pure calcium sulfate cement and nanocomposites were identified by Fourier Transform Infrared Spectroscopy (FTIR) in transmission mode. Ten milligrams of the powdered sample were mixed with 800 mg of ground spectroscopic grade KBr and pressed to make a transparent KBr pellet. The Infrared spectra were measured in the range of 4,000–400 cm^{-1} at a resolution of 2 cm^{-1} using BRUKER VECTOR 33 spectrometer.

2.2.5 Microstructures

Surface morphology of the cement specimens was assessed by scanning electron microscopy (SEM, Stereoscan S 360 Cambridge) which operated at accelerating voltage of 20 kV. Because of poor conductivity of the samples, the surface of each specimen was coated with a thin layer of gold before testing.

2.2.6 Qualitative disintegration and weight loss

The washout behavior of each cement formulation was qualitatively showed as follows: Disc-shaped specimens (10 mm in diameter and 5 mm in height) fabricated from the cement paste were immersed in 50 ml of SBF solution immediately after setting and left at 37°C for 3 days. Then visual quality of the samples was recorded with a digital camera (Canon sd1100is).

To measure weight loss of each sample, disc-shaped specimen was fabricated as described above, dried at room temperature, weighed and immersed in simulated body fluid at 37°C. After different time intervals, the sample was removed from the SBF solution, dried at room temperature and its weight loss was determined according to the following expression:

$$\text{Weight loss } (\%) = 100\ (w_1 - w_2)/w_1 \quad (1)$$

where w_1 was weight of sample before soaking and w_2 was weight of the sample after soaking in the SBF solution.

2.2.7 In vitro bioactivity

In this part of the study, to evaluate apatite-formation ability of the cements (that is called "bioactivity" by some authors), disc-shaped specimens of both calcium sulfate/nanoapatite and calcium sulfate/nanoapatite/nanosilica were separately immersed in the SBF solution (0.4 g/100 ml) and kept at 37°C for 9 days. The SBF solution was replaced with fresh solution every 24 h. After each day, Ca and Si concentration of the extracted SBF solution was checked by inductively coupled plasma-atomic emission spectroscopy. After 9 days, the surface morphology of the samples was analyzed by using the SEM instrument as described in Sect. 2.2.5.

2.2.8 Cell viability and alkaline phosphatase activity

The human osteosarcoma (G-292) cells were prepared from national cell bank of Iran (NCBI C 116). The cells were cultured in tissue culture polystyrene flasks (Falcon, USA) at 37°C under 5% CO_2 atmosphere in Dulbecco's modified Eagle's medium (DMEM) with L-glutamine, supplemented with 10% fetal bovine serum and antimycotic antibiotic (100 units penicillin G sodium, 100 mg streptomycin sulfate, and 0.25 mg amphotericin B in saline) and harvested after the treatment with 0.05% trypsin–EDTA.

The pure calcium sulfate, C-H and nanosilica added composite extracts were used in full culture medium according to International Standard Organization (ISO/EN 10993-5) [18]. The dissolution extracts of various cements were prepared by adding cements in powdered form to serum free α-MEM culture medium at a ratio of 200 mg/ml (powder to medium). After incubation at 37°C for 24 h, the mixture was centrifuged and filtered through a membrane. The pure extract (which was considered 100 vol.%) was diluted to 50 and 25 vol.% by adding serum free α-MEM and hence serial dilutions were employed for cell response assessment. The diluted extracts were sterilized using 0.22 μm filter and used in the cell culture experiments. The concentration of Ca and Si ions in diluted extracts were measured using inductively coupled plasma technique. The osteoblastic cells were seeded at a density of 1.3×10^4 cells/well into 96-well plate and incubated for 24 h. After cell adhesion, the culture medium was removed and each serial dilution supplemented with 20% fetal calf serum (FCS) was added to the plate inoculating G-292 cells. The culture medium supplemented with 10% FCS without addition of extracts was used as a blank control (control group). Then, the cells were incubated at 37°C in 5% CO_2 for 2, 5, 7 and 14 days. The medium was removed every 3 days and fed with fresh one (including dilution or control medium).

The mitochondria activity of the bone cells after exposure to various extracts was determined by colorimetric assay, which detected the conversion of 3-(4,5 dimethylthiazol-2yl)-2,5-diphenyltetrazolium bromide (MTT, Sigma) to formazan.

After each period, MTT was dissolved in phosphate buffered saline at 5 mg/ml and 20 μl was added to each well reaching a final concentration of 0.5 mg MTT/ml. After an incubation time of 4 h, unreacted dye was removed by aspiration and the purple formazan product

was dissolved in 200 µl/well dimethylsulfoxide and quantified by a plate reader (BIO-TEK Elx 800, Highland park, USA) at wavelengths of 570 nm. The cell numbers were calculated based on standard curve prepared from the results of cell viability test performed by different known cell densities.

Alkaline phosphatase (ALP) activity was determined according to Lowry et al. [19] with *p*-nitrophenyl as the substrate. Sample volumes of 0.1 ml were added to 0.1 ml *p*-nitrophenyl phosphate (Sigma) in 0.1 M glycine (pH = 13.0), and incubated at 37°C for 30 min. The enzymatic reaction was stopped by addition of 0.3 ml of 0.25 N NaOH. Enzyme activity was quantified by absorbance measurements at 410 nm for the amount of *p*-nitrophenol liberated [20]. The obtained absorbance was normalized by the amount of cell presented at each time.

2.3 Statistical analysis

Data were processed using Microsoft Excel 2003 software and the results were produced as mean ± standard deviation of at least four experiments. Significance between the mean values was calculated using standard software program (SPSS GmbH, Munich, Germany) and the $P \leq 0.05$ was considered significant.

3 Results and discussion

3.1 Initial setting time and mechanical strength

In the present paper, nanosilica as a colloidal system was used to improve undesirable characteristics of calcium sulfate/nanostructured apatite nanocomposite cement including long setting time, low mechanical strength, washout and lack of bioactivity. Calcium sulfate is used as reactive ingredient of the cement to react with water (a hydraulic reaction) and produce calcium sulfate dihydrate which is responsible for the cement strength while nanoapatite is used as an osteoconductive filler.

The apatite phase was prepared in the SBF solution from the hydraulic reactions and conversion of calcium phosphate cement reactants (i.e. TTCP and DCPD), because it has been proved that such apatite phase mimics inorganic phase of bones in terms of crystallinity and stoichiometry.

In our pilot stage, various nanocomposite cements were made with different concentrations of colloidal silica (1, 5, 10 and 20%). Since the best results in terms of setting time, compressive strength and washout were achieved for the cement made by suspension of 20 wt% of colloidal silica, it was chosen for further studies. Note that the goal of this study was not to evaluate the influence of colloidal silica concentration on basic properties of C-H cement though it can be considered as a research topic.

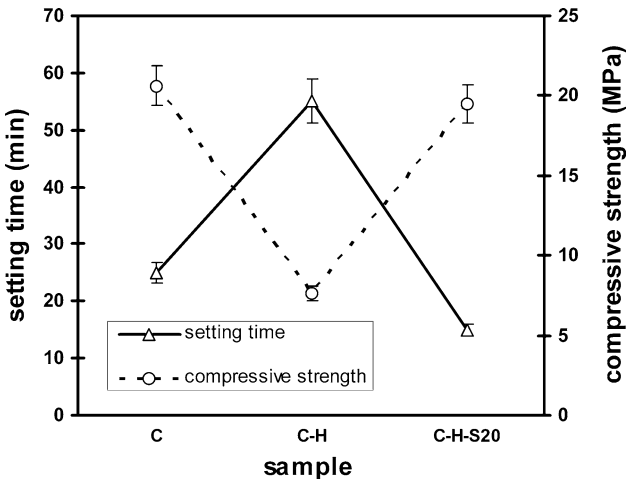

Fig. 1 The initial setting time and compressive strength of different calcium sulfate-based bone cements

It has been shown in Fig. 1 how setting time and compressive strength of calcium sulfate-nanoapatite cement are influenced by adding colloidal silica. The values of pure calcium sulfate cement are also reported for comparison. The initial setting time of pure calcium sulfate cement is about 25 min, an acceptable time for surgical operations, which increases to ~55 min when 40 wt% of the hemihydrate phase ($CaSO_4 \cdot 0.5\ H_2O$) is replaced with nanoapatite. When solution of nanosilica is used as liquid phase of nanocomposite, the initial setting time is recovered again and reaches to about 17 min (for C-H-S20). It is a promising time for surgical operations. The same condition is also observed for compressive strength. While compressive strength failed from ~21 MPa for pure calcium sulfate cement to ~7 MPa for C-H, it is recovered to the value of ~19 MPa by using 20% nanosilica additive (C-H-S20).

From the results, it is clear that both setting time and mechanical strength of the calcium sulfate tend to fail by adding nanoapatite because of (i) decreased concentration of the reactive ingredient (calcium sulfate) leading to reduced matrix entanglement and (ii) presence of the filler particles between the rodlike crystals which decreases their physical bonding strength.

Colloidal silica is a suspension of fine amorphous, nonporous, and typically spherical silica particles in an aqueous phase in which the particle size ranges from 30 to 100 nm. It is currently used as a high temperature binder, catalyst and coagulating agent in ceramic industries and as a concrete densifier in building mortars. The subunits of colloidal silica particles are usually un-joined $Si(OH)_4$. Hydrogen ions from the surfaces of colloidal silica particles tend to dissociate in aqueous solution and thus, the

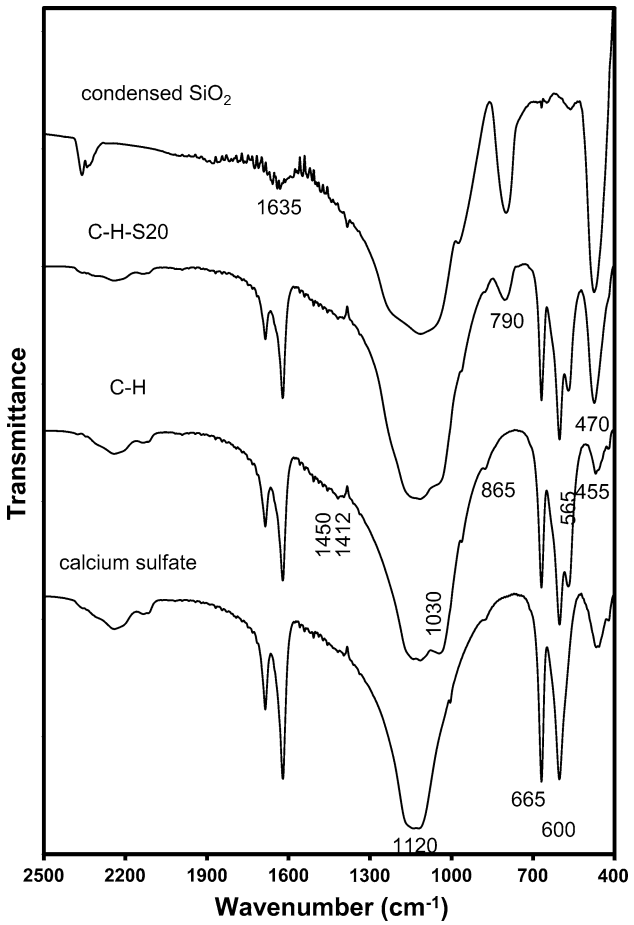

Fig. 2 The FTIR spectra of pure calcium sulfate cement and C-H nanocomposite in comparison with C-H-S20 nanocomposite and condensed SiO_2

ions existed at the surface is OH^-, yielding an electrostatically dispersed suspension.

Thus, it is suggested that the gypsum crystals produced from the hydrolysis of $CaSO_4{\cdot}0.5H_2O$ particles (Eq. 2) are formed among the colloidal silica particles and simultaneously the colloidal silica particles interact together and polymerize to a 3D network of Si–O–Si groups (Eq. 3) when the liquid of the cement is consumed by the hemihydrate phase to form dihydrate one (see Fig. 2, the stretching band at 790 cm^{-1} corresponding to Si–O–Si (siloxane) group in silica tetrahedra):

$$CaSO_4{\cdot}0.5H_2O + 1.5H_2O = CaSO_4{\cdot}2H_2O \quad (2)$$

$$Si{-}OH + Si{-}OH = Si{-}O{-}Si + H{-}OH \quad (3)$$

Condensation of the colloidal silica to siloxane occurs through a gelling mechanism [21] that improves setting time of the nanocomposite cement. The compressive strength is a misconstrue-dependent property. The role of colloidal silica in modifying C-H nanocomposite microstructure is described in the next section.

3.2 Structural properties of the cements

FTIR spectra of pure calcium sulfate; C-H and C-H-S20 specimens are compared in Fig. 2. The FTIR spectrum of condensed SiO_2 is also shown. In the spectra of all samples, the bands appeared at 600, 665 and 1,120 cm^{-1} are assigned to stretching modes of SO_4^{2-} group [10]. For nanocomposite spectra, the bands appeared around 455,565 and 1,030 cm^{-1}correspond to stretching modes of PO_4 group in the apatite lattice. In C-H-S20 specimen, the bands at 790 and 470 cm^{-1} are due to Si–O–Si symmetric stretching in the ring structure of SiO_4 tetrahedra and Si–O–Si bending vibrations, respectively [22]. These bands are clearly observed in the FTIR spectrum of condensed SiO_2. Regarding to the spectrum of condensed silica, it can be stated that colloidal silica in nanocomposite cement has polymerized to SiO_2. Note that in the silica-containing specimen, the bands appeared at 455 and 470 cm^{-1} have overlap and thus an amplified band with increased intensity is observed.

Figure 3 shows the X-ray diffraction patterns of set C, C-H and C-H-S20 cements specimens. The XRD pattern of cement set by mixing CSH powder and suspension of 20 wt% of colloidal silica (that is called C-S20 here) is also shown for comparison. The patterns of both C and (C-S20) cements exhibit the characteristic peaks of gypsum (calcium sulfate dihydrate, ICDD #33-0311) and no further phases are found in the composition of C-S20. In addition to gypsum, apatite phase with broadened peaks is also observed in the patterns of nanocomposite cements. The intensities of apatite peaks are not proportional to its content in the cement composition because of its poor crystallinity. Furthermore, in nanosilica-containing samples (C-S20 and C-H-S20), gypsum phase shows an increase in intensity of peak at $2\theta = 20.7°$ responding to 021crystal planes. Thus it seems that silicate ions induced a proffered direction of growth of gypsum crystals during setting. Compared to pure gypsum, in other samples, i.e. C-H, C-H-S20 and C-S20, XRD peaks of gypsum phase reveal a shift to lower diffraction angles. This suggests that PO_4^{3-} or SiO_4^{4-} ions may be incorporated into the lattice structure of gypsum.

The scanning electron micrographs of pure calcium sulfate and nanocomposites with and without nanosilica additive are shown in Fig. 4. Microstructure of pure calcium sulfate comprises of many rodlike crystals tightly entangled to each others. In C-H cement, the thicker rodlike crystals are observed compared to C, meanwhile they have been covered with aggregated apatite particles. Additionally, C-H exhibits more porous microstructure in comparison to C. When nanosilica is used in the nanocomposite cement, a compacted microstructure is achieved in which a condensed phase embeds gypsum crystals

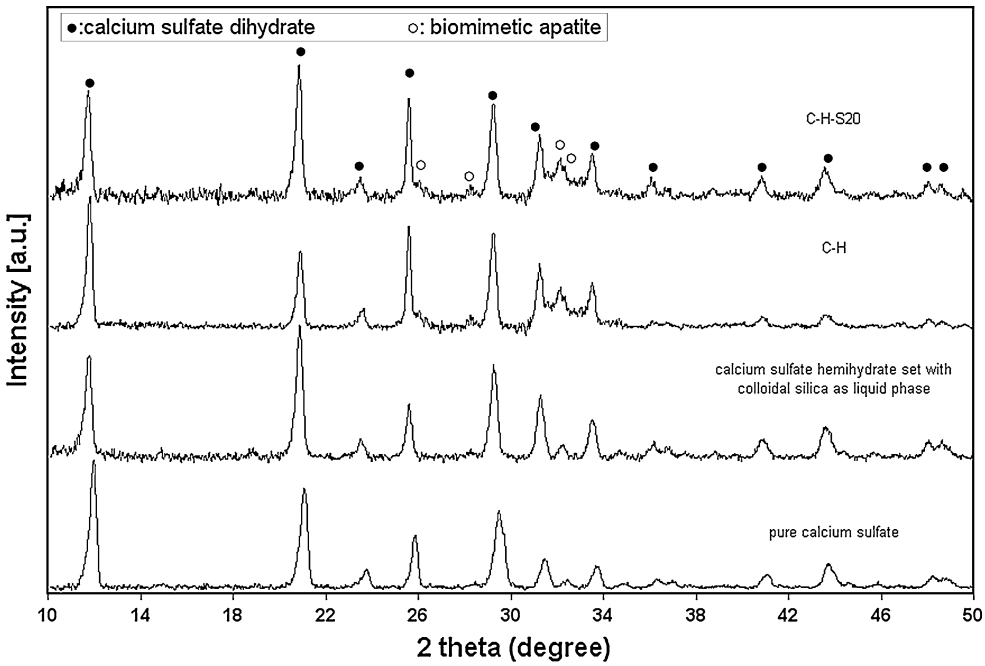

Fig. 3 The XRD patterns of the set pure calcium sulfate, C-H and C-H-S20 cements. The XRD pattern of a hardened cement made by mixing calcium sulfate hemihydrates powder and suspension of colloidal silica is also shown for comparison

covered by apatite aggregates and fills the spaces (pores) between them. It can explain the improved compressive strength of C-H-S20 compared to C-H nanocomposite cement.

3.3 Washout behavior and weight loss

Figure 5 shows the effect of adding colloidal silica on the washout behavior of C-H nanocomposite, qualitatively. Pure calcium sulfate cement exhibits slight disintegration when is kept in the SBF medium for 3 days (Fig. 5a). The addition of apatite filler to calcium sulfate accelerates dissociation of the obtained composite in physiologic medium due to dissociation of the filler phase (Fig. 5b). Undesirable washout of C-H is completely controlled by adding nanosilica to its composition so that no separated particles are observed in the surrounding medium of the soaked C-H-S20 (Fig. 5c). It is suggested that the condensed phase that fills spaces between the calcium sulfate dihydrate crystals or covered them can control washout behavior of the cement.

Figure 6 shows the loss in weight of different specimens against immersion time. Duration of weight loss is observed for all samples by elapsing the soaking time. In all soaking periods, the maximum weight loss belongs to C-H so that more than 80% of its initial weight is lost after 15 days; however the weight loss of C-H-S20 at the end of evaluating period is respectively 20 and 45% lower than that of C and C-H. This clearly shows the function of nanosilica in controlling bioresorption and washout behavior of the nanocomposites.

Calcium sulfate is a fast biodegradable material. It degrades in body through dissolution process when it is subjected to dynamic fluids (such as body fluids). It has been proved that high level of dissolved Ca ions in extracellular matrix affect gene expression and thus ALP activity resulting in rapid bone healing process [23]. However, when calcium sulfate is incorporated with apatite particles another phenomenon occurs that may fail efficacy of resultant composite despite of beneficial role of each component alone. It is structural instability of the composite when contacting with fluid currents. In this situation the material does not degrade gradually through dissolution process but immediately destroys by disintegration of its components into debris and unbounded particles. This behavior is known as washout. Due to the washout behavior, the bone cement leaves the defect site in early stage of healing process meanwhile the resultant debris can migrate to surrounding tissues leading to inflammatory reactions [24]. In this study it has been shown that the washout behavior of calcium sulfate-apatite composites is completely controlled by using nanosilica additive. When nanosilica is used in the composition of calcium sulfate-apatite composite, biodegradation can happen through dissolution, i.e. by introducing ions not particles and it is obvious from the literatures that Ca^{2+} accompanied with Si ions have a positive effect on cell functions [25].

3.4 In vitro apatite-formation ability

Another surprising effect of nanosilica on C-H nanocomposite cement is its ability of apatite-formation in SBF

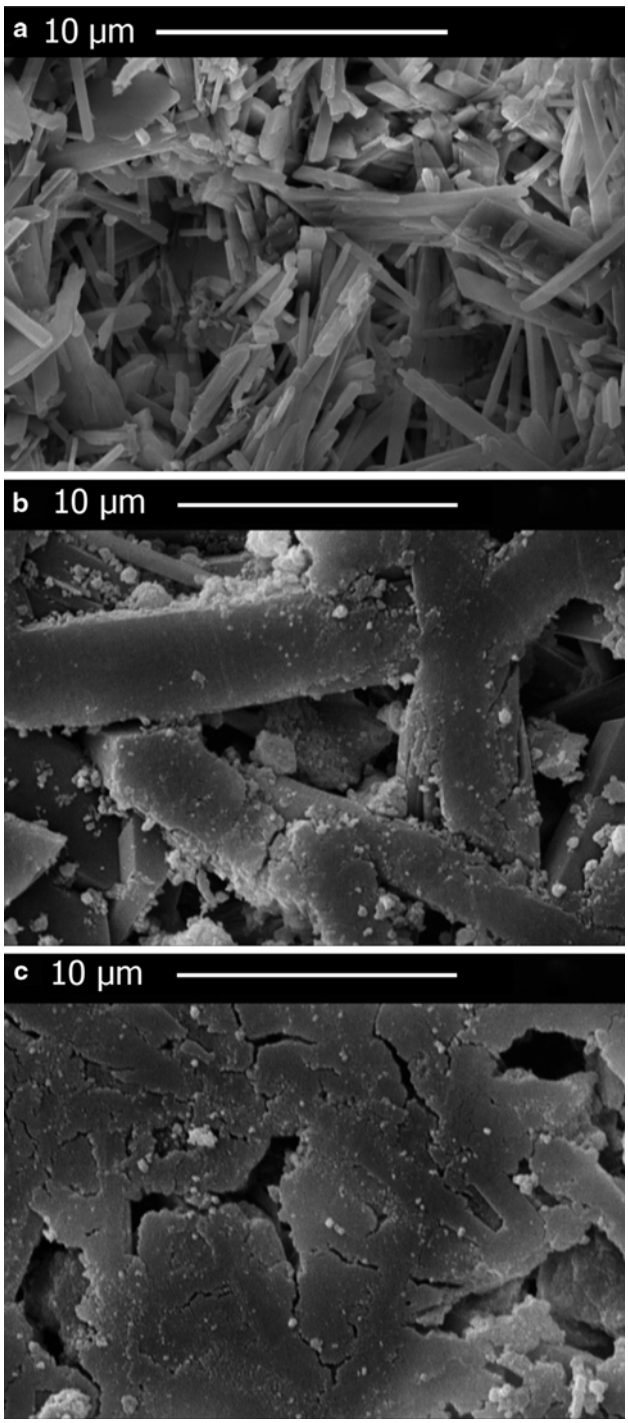

Fig. 4 The SEM micrographs of pure calcium sulfate cement (**a**), C-H (**b**) and C-H-S20 (**c**) nanocomposite after setting

solution. The surface morphologies of C-H and C-H-S20 specimens soaked in the SBF solution for 9 days have been compared in Fig. 7. The only observed difference between the surface morphology of C-H specimen before (Fig. 4b) and after (Fig. 7a) soaking in the SBF solution is the destruction and dissolution of gypsum crystals due to the soaking process. However, the surface morphology of the soaked nanosilica-containing nanocomposite is completely different from that of non-immersed one. Formation of a layer with ball-like morphology is observed over the surfaces of the soaked C-H-S20 specimen. It is well known that such morphology corresponds to bone-like apatite layer produced onto the surfaces of a bioactive specimen during immersion in a physiologic solution (e.g. SBF) [26].

The authors suggest that the bioactivity of the silica-containing nanocomposite cement originates from the presence of condensed colloidal silica-derived SiO_2 phase in the cement structure. It has been discussed in literatures [27] that two processes of dissolution and precipitation can occur during immersion of bioactive materials in the SBF solution. These phenomena may induce formation of calcium phosphate layer onto the material surfaces. Although the solubility of surfaces is essential for precipitation of biomimetic apatite layer, the chemistry of surface is also important [28]. It has been shown that surfaces with Si–OH or Ti–OH groups are susceptible sites for the calcium phosphate nucleation [29]. The Si–OH groups can be formed onto the surfaces of SiO_2-containing bioactive materials or sol gel processed silica [30] through the exchanging process between the H^+ cations from the physiologic solution and Ca^{2+} or other cations existed in the material surfaces. The mechanisms of apatite layer formation on the surfaces of bioactive materials have been well discussed by authors [31]. Chemistry of SBF solution assists to determine kinetic of apatite formation on bioactive surfaces.

Table 2 presents, ΔCa, the difference between Ca^{2+} concentrations of the fresh SBF and the specimen-containing SBF up to 9 days of soaking. The amount of Si released from the silica-containing specimens is also shown (values in parenthesis). In all evaluating days, level of Ca release from the C-H nanocomposite is lower than pure calcium sulfate (due to the lower solubility of apatite compared to calcium sulfate) and further decrease in Ca^{2+} concentration is found for nanosilica-containing cements. Since there is a direct relationship between Ca concentration and water solubility of samples, it can be stated that the solubility of C-H decreases with incorporating nanosilica additive. For C-H-S20 specimen, when ΔCa decreases sharply at day 9 and approaches to zero, it means that the Ca ions have been extensively consumed for precipitation of apatite phase on sample surfaces. It reveals an active precipitation process during the last evaluating periods. The concentration of Si ions in the SBF solution is proportional to its loading content in the cement formulation, i.e. the higher colloidal silica in the cement composition, the higher Si ions in the SBF solution. A reduced Si release is observed for both silica-containing cements after 9 days of immersion probably due to inhibitory effect of the formed apatite layer.

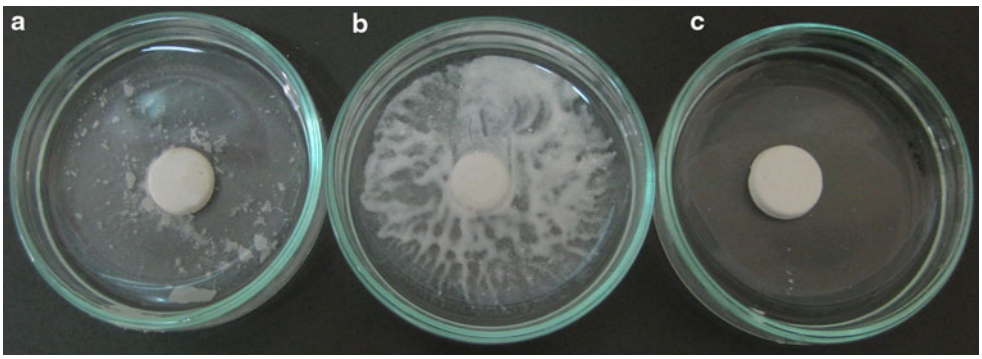

Fig. 5 Comparison between disintegration of various calcium sulfate-based cements when soaking in SBF solution for 3 days: **a** C, **b** C-H , and **c** C-H-S20

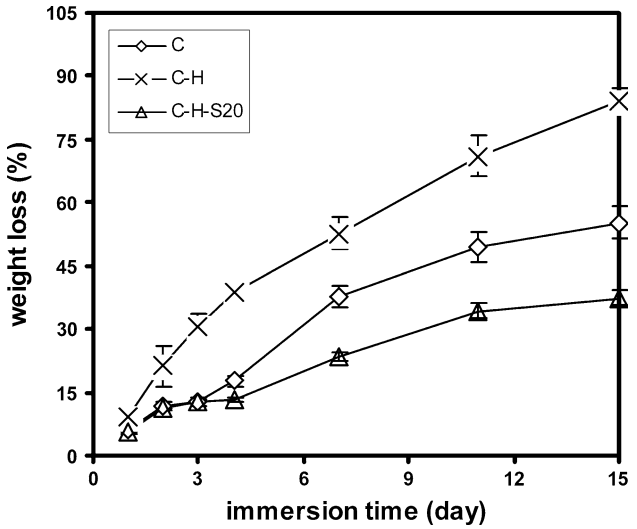

Fig. 6 The weight loss of calcium sulfate-based cements as a function of time

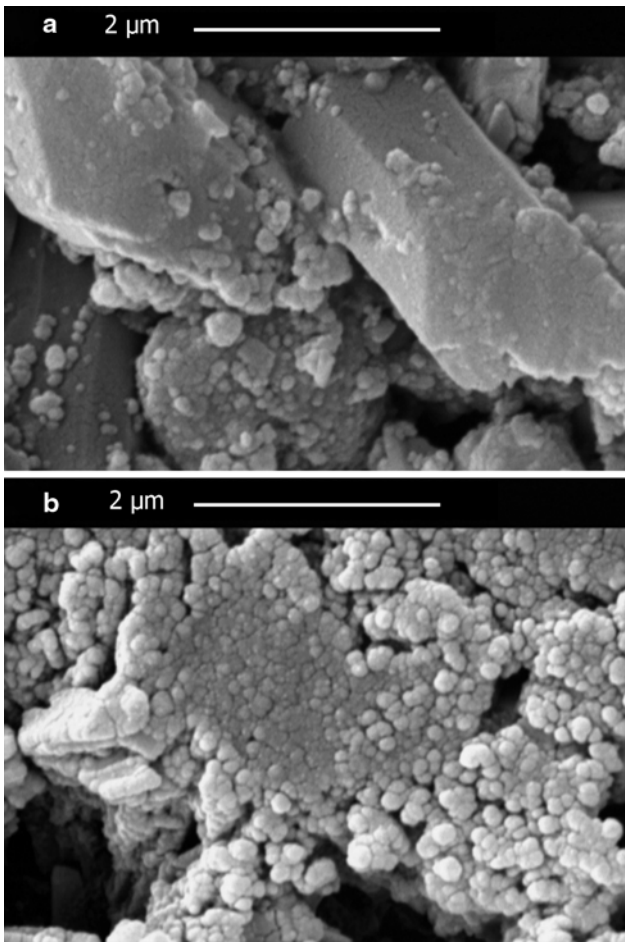

Fig. 7 The surface morphologies of C-H (**a**) and CS-H-S20 (**b**) cements after soaking in the SBF solution for 9 days

3.5 Cell proliferation and ALP activity

The extraction method was selected for cell culture evaluation, because if direct contact procedure had been chosen, C-H samples would have suffered from disintegration upon confronting with culture medium. Table 3 represents Ca and Si concentration of various extracts diluted to different concentrations. The concentration of Ca and Si (in C-H-S20 sample) ions decreased by diluting the primary extract (100 vol.%) to 50 and 25 vol.% of its initial concentration. Figure 8 shows the results of cell proliferation in the presence of various extracts [C (Fig. 8a), C-H composite (Fig. 8b) and C-H-S20 (Fig. 8c)] with different concentrations. For all specimens, proliferation of the osteoblastic cells increases with increasing cell culture time. G-292 proliferation is comparable when cells are cultured with different extracts for 2 days. However, in other days, for all experimental groups, the number of viable cells cultured with extracts is significantly ($P < 0.05$) higher than that of control group (blank) regardless of extract concentration. At the same culture periods, there is no significant difference between the numbers of viable cells cultured with various dilutions of each extract. Moreover, difference between the cell numbers of various extracts with the same diluting concentrations is not statistically significant ($P > 0.05$).

Table 2 Difference between Ca concentrations of the fresh SBF and the specimen-containing SBF after each evaluating period (values are presented in mg/l unit)

	Day 1	Day 2	Day 3	Day 7	Day 9
C	206.4[a]	256.4	259.7	462.4	288.6
C-H	179.9	201.7	230.6	290.3	148.5
C-H-S20	171.3 (7.6)[b]	176.7(7.1)	106.7 (5.9)	67.6 (4.1)	6.2 (0.9)

[a] The values have been normalized based on the weight of specimens

[b] The value in parentheses is concentration of Si ions released from the nanosilica-added specimens into the SBF solution

Table 3 The Ca and Si ion concentrations of various sample extracts used in cell culture experiment (values in ppm)

Sample code	Ion	Extract concentration			
		Blank	100	50	25
C	Ca	142	245	136	87
	Si	0	0	0	0
C-H	Ca	142	186	102	75
	Si	0	0	0	0
C-H-S20	Ca	142	174	95	54
	Si	0	9.5	5.3	2.6

Cytotoxicity of calcium sulfate is in challenge among researchers. While some authors have stated that calcium sulfate exhibits a transient cytotoxic behavior [13] many authors have expressed that calcium sulfate is a biocompatible material [23, 32]. Several parameters such as material purity (presence of impurities), cell type and culture medium can be mentioned as origin of these contradictions. In this study, no signs of cytotoxicity were observed for pure calcium sulfate cement.

Alkaline phosphatase activity of the osteoblasts contacted with various concentrations of different extracts is shown in Fig. 9. Evidently, for all groups, the ALP activity increases significantly with increasing culture time up to 7th day and then inhibited at 14th day. Decrease in ALP activity may be related to the cell confluence [26]. As a common statement, the average value of ALP of the cells cultured with the cement extracts is higher than that of control group and the significance depends on extract concentration (in fact Ca concentration). For example, the ALP activity of the cells cultured without any extract for 5 and 7 days is comparable to that of pure calcium sulfate extract with concentration of 25 vol.% whereas it is significantly lower than that of calcium sulfate extract with

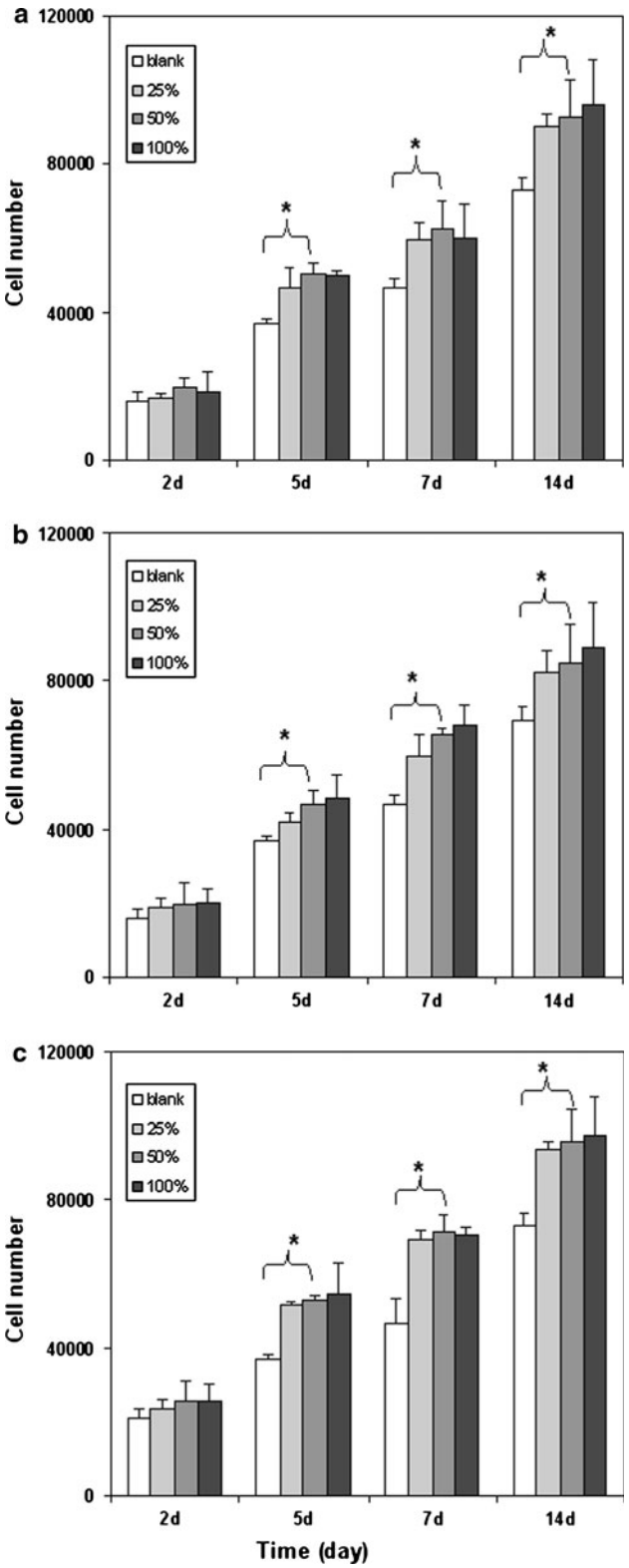

Fig. 8 Proliferation of the osteoblastic cells cultured with different concentrations of various sample extracts: **a** pure calcium sulfate, **b** C-H nanocomposite, and **c** C-H-S20 nanocomposite (* $P < 0.05$)

concentrations of 50 and 100 vol.%. It is obvious from the results that ALP activity is dependent on Ca concentration of the medium. However, the interesting finding is that ALP activity of osteoblastic cells is improved in the presence of Si ions. Concentration of Si ions is also important in cell enzymatic reactions. As shown in Fig. 9c, the level of ALP increases with increasing in extract concentration (Si and Ca concentration) and difference between absorbance number of different dilutions is statistically significant ($P < 0.05$). When comparing ALP activity of the cells cultured with different extracts for 5 and 7 days (Fig. 9a–c), it is found that ALP of the cells cultured with C-H-S20 extract (even at low concentrations) is significantly higher than that of pure calcium sulfate and C-H. In other words, the high concentration of Ca and Si ions can increase G-292 activity and with incorporation of Si ions even low concentration of Ca ions enhances cell activity.

Alkaline phosphatase is known as an early osteoblastic differentiation marker and is produced by the cells showing mineralized extracellular matrix [33].

The superior biological performance of Si-containing hydroxyapatite and tricalcium phosphate has been well documented in literatures [34–37]. In this study it is suggested that the better ALP activity of the osteoblasts cultured with C-H-S20 extracts is due to the presence of silicon ions released from the cements. In addition to characteristics such as setting time, compressive strength and washout behavior, our experience showed that the rheological and handling properties of C-H nanocomposite cement can be modified by adding nanosilica which is in our next research program.

4 Conclusions

The results showed that colloidal silica is a promising additive to modify undesirable characteristics of calcium sulfate/nanostructured apatite bone cement. The appropriate setting time, enough compressive strength (comparable to cancellous bone) and structural stability of calcium sulfate cement lost by adding nanoapatite filler can be thoroughly recovered by using colloidal silica in the cement composition. The bioresorption behavior of the cement prepared by colloidal silica is more controllable than that of pure calcium sulfate and nanocomposite cement prepared by distilled water. In addition to enhanced physical properties of silica-containing cement, this system exhibits ability of apatite formation over its surfaces when soaking in simulated body fluid solution. Furthermore, the use of colloidal silica in the cement composition not only maintains proliferation of osteoblastic cells but also increases their ALP activity and thus can be successfully used as bone filler after passage of the corresponding in vivo tests.

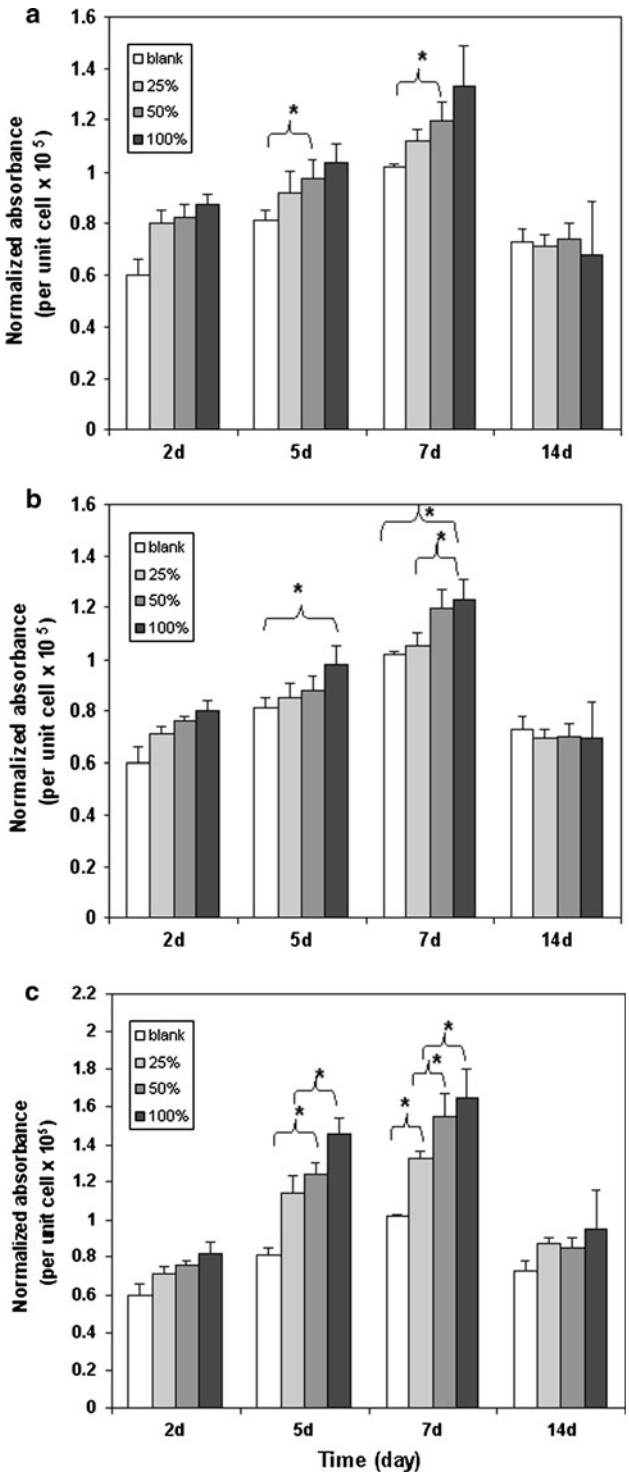

Fig. 9 The ALP activity of G-292 cells cultured with different concentrations of various cement extracts: **a** pure calcium sulfate, **b** C-H nanocomposite, and **c** C-H-S20 nanocomposite (* $P < 0.05$)

Acknowledgment The authors wish to appreciate Pasteur institute of Iran for cell culture experiments.

References

1. Stubbs D, Deakin M, Chapman-Sheath P, Bruce W, Debes J, Gillies RM, Walsh WR. In vivo evaluation of resorbable bone graft substitutes in a rabbit tibial defect model. Biomaterials. 2004; 25:5037–44.
2. Tay BK, Patel VV, Bradford DS. Calcium sulfate- and calcium phosphate-based bone substitutes mimicry of the mineral phase of bone. Orthop Clin North Am. 1999;30:615–23.
3. Delloye C, Cnockaert N, Cornu O. Bone substitutes in 2003: an overview. Acta Orthop Belg. 2003;69:1–8.
4. Ginebra MP, Traykova T, Planell JA. Calcium phosphate cements as bone drug delivery systems: a review. J Control Release. 2006;113:102–10.
5. Habib M, Baroud G, Gitzhofer F, Bohner M. Mechanisms underlying the limited injectability of hydraulic calcium phosphate paste part II: particle separation study. Acta Biomater. 2010;6:250–6.
6. Alexander DI, Manson NA, Mitchell MJ. Efficacy of calcium sulfate plus decomposition bone in lumbar and lumbosacral spinal fusion: preliminary results in 40 patients. Can J Surg. 2001; 44:262–6.
7. Pecora G, De Leonardis D, Ibrahim N, Bovi M, Cornelini R. The use of calcium sulphate in the surgical treatment of a 'through and through' periradicular lesion. Int Endod J. 2001;34:189–97.
8. Guarnieri R, Pecora G, Fini M, Aldini NN, Giardino R, Orsini G, Piattelli A. Medical grade calcium sulfate hemihydrate in healing of human extraction sockets: clinical and histological observations at 3 months. J Periodontol. 2004;75:902–8.
9. Kelly CM, Wilkins RM, Gitelis S, Hartjen C, Watson JT, Kim PT. The use of a surgical grade calcium sulfate as a bone graft substitute. Clin Orthop. 2001;382:44–50.
10. Doadrio JC, Arcos D, Cabañas MV, Vallet-Regí M. Calcium sulphate-based cements containing cephalexin. Biomaterials. 2004;25:2629–35.
11. Coetzee AS. Regeneration of bone in the presence of calcium sulfate. Arch Otolaryng. 1980;106:405–9.
12. Robinson D, Alk D, Sandbank J, Farber R, Halperin N. Inflammatory reactions associated with a calcium sulfate bone substitute. Ann Transplant. 1999;4:91–7.
13. Rauschmann MA, Wichelhaus TA, Stirnal V, Dingeldein E, Zichner L, Schnettler R, Alt V. Nanocrystalline hydroxyapatite and calcium sulphate as biodegradable composite carrier material for local delivery of antibiotics in bone infections. Biomaterials. 2005;26:2677–84.
14. Hesaraki S, Moztarzadeh F, Nezafati N. Evaluation of a bioceramic-based nanocomposite material for controlled delivery of a non-steroidal anti-inflammatory drug. Med Eng Phys. 2009;31: 1205–13.
15. Hesaraki S, Moztarzadeh F, Nemati R, Nezafati N. Preparation and characterization of calcium sulfate-biomimetic apatite nanocomposites for controlled release of antibiotics. J Biomed Mater Res B. 2009;91:651–61.
16. Hesaraki S, Moztarzadeh F, Sharifi D. Formation of interconnected macropores in apatitic calcium phosphate bone cement with the use of an effervescent additive. J Biomed Mater Res A. 2007;83:80–7.
17. Kokubo T, Kushitani H, Sakka S, Kitsugi T, Yamamuro TJ. Solutions able to reproduce in vivo surface-structure changes in bioactive glass-ceramic A-W. J Biomed Mater Res. 1990;24: 721–34.
18. ISO/EN 10993-5. Biological evaluation of medical devices—part 5 tests for cytotoxicity, in vitro methods: 8.2 tests on extracts.
19. Lowry OH, Roberts NR, Wu ML, Hixon WS, Crawford EJ. The quantitative histochemistry of the brain. J Biol Chem. 1954;207: 19–37.
20. Elgendy HM, Norman ME, Keaton AR, Laurencin CT. Osteolike cell (MC3T3–E1) proliferation on biorodible polymers: an approach towards the development of a bone-bioerodible polymer composite material. Biomaterials. 1993;14:263–9.
21. Iler RK. The chemistry of silica, solubility, polymerisation, colloid and surface properties and biochemistry. New Jersey: Wiley; 1979.
22. Jeon HJ, Yi SC, Oh SG. Preparation and antibacterial effects of Ag-SiO2 thin films by sol–gel method. Biomaterials. 2003;24: 4921–8.
23. Lazáry A, Balla B, Kósa JP, Bácsi K, Nagy Z, Takács I, Varga PP, Speer G, Lakatos P. Effect of gypsum on proliferation and differentiation of MC3T3–E1 mouse osteoblastic cells. Biomaterials. 2007;28:393–9.
24. Alliot-Licht B, Gregoire M, Orly I, Menanteau J. Cellular activity of osteoblasts in the presence of hydroxyapatite: an in vitro experiment. Biomaterials. 1991;12:752–6.
25. Boher M. Silicon-substituted calcium phosphates—a critical view. Biomaterials. 2009;30:6403–6.
26. Wong KL, Wong CT, Liu WC, Pan HB, Fong MK, Lam WM, Cheung WL, Tang WM, Chiu KY, Luk KD, Lu WW. Mechanical properties and in vitro response of strontium-containing hydroxyapatite/polyetheretherketone composites. Biomaterials. 2009;30: 3810–7.
27. Balamurugan A, Balossier G, Michel J, Kannan S, Benhayoune H, Rebelo AH, Ferreira JM. Sol gel derived SiO_2-CaO-MgO-P_2O_5 bioglass system—preparation and in vitro characterization. J Biomed Mater Res B. 2007;83:546–53.
28. Habibovic P, Barrere F, van Blitterswijk C, de Groot K, Layrolle P. Biomimetic hydroxyapatite coatings on metal implants. J Am Chem Soc. 2002;85:517–22.
29. Miyai F, Iwai M, Kokubo T. Chemical surface treatment of silicone for inducing its bioactivity. J Mater Sci Mater Med. 1998; 9:61–5.
30. Uchida M, Kim H, Kokubo T. Apatite forming ability of sodium containing titania gels in a simulated body fluid. J Am Ceram Soc. 2001;84:2969–74.
31. Salinas AJ, Martin AI, Vallet-Regi M. Bioactivity of three CaO–P_2O_5–SiO_2 sol–gel glasses. J Biomed Mater Res A. 2002;61: 524–32.
32. Palmieri A, Pezzetti F, Brunelli G, Scapoli L, Lo Muzio L, Scarano A, Martinelli M, Carinci F. Calcium sulfate acts on the miRNA of MG63E osteoblast-like cells. J Biomed Mater Res B. 2008;84:369–74.
33. Stein GS, Lian JB, Owen TA. Relationship of cell growth to the regulation of tissue-specific gene expression during osteoblast differentiation. FASEB J. 1990;4:3111–23.
34. Mastrogiacoma M, Muraglia A, Komlev V, Peryin F, Rustichelli F, Crovace A. Tissue engineering of bone: search for a better scaffold. Orthod Craniofac Res. 2005;8:277–84.
35. Pietak A. The role of silicon in Si-TCP bioceramics: a material and biological characterization. Kingston: Queen's University; 2004.
36. Hing K, Revell P, Smith N, Buckland T. Effect of silicon level on rate, quality and progression of bone healing within silicate substituted porous hydroxyapatite scaffolds. Biomaterials. 2006;27:5014–26.
37. Pietak AM, Reid JW, Stott MJ, Sayer M. Silicon substitution in the calcium phosphate bioceramics. Biomaterials. 2007;28: 4023–32.